



# Pre-treatment CT-based radiomics nomogram for predicting microsatellite instability status in colorectal cancer

Qian Pei<sup>1</sup> · Xiaoping Yi<sup>2,3</sup> · Chen Chen<sup>4</sup> · Peipei Pang<sup>5</sup> · Yan Fu<sup>2,3</sup> · Guangwu Lei<sup>2</sup> · Changyong Chen<sup>2</sup> · Fengbo Tan<sup>1</sup> · Guanghui Gong<sup>6</sup> · Qingling Li<sup>6</sup> · Hongyan Zai<sup>1</sup> · Bihong T. Chen<sup>7</sup>

Received: 4 December 2020 / Revised: 23 May 2021 / Accepted: 8 June 2021 / Published online: 13 July 2021

© European Society of Radiology 2021

## Abstract

**Objectives** Stratification of microsatellite instability (MSI) status in patients with colorectal cancer (CRC) improves clinical decision-making for cancer treatment. The present study aimed to develop a radiomics nomogram to predict the pre-treatment MSI status in patients with CRC.

**Methods** A total of 762 patients with CRC confirmed by surgical pathology and MSI status determined with polymerase chain reaction (PCR) method were retrospectively recruited between January 2013 and May 2019. Radiomics features were extracted from routine pre-treatment abdominal pelvic computed tomography (CT) scans acquired as part of the patients' clinical care. A radiomics nomogram was constructed using multivariate logistic regression. The performance of the nomogram was evaluated using discrimination, calibration, and decision curves.

**Results** The radiomics nomogram incorporating radiomics signatures, tumor location, patient age, high-density lipoprotein expression, and platelet counts showed good discrimination between patients with non-MSI-H and MSI-H, with an area under the curve (AUC) of 0.74 [95% CI, 0.68–0.80] in the training cohort and 0.77 [95% CI, 0.68–0.85] in the validation cohort. Favorable clinical application was observed using decision curve analysis. The addition of pathological characteristics to the nomogram failed to show incremental prognostic value.

**Conclusions** We developed a radiomics nomogram incorporating radiomics signatures and clinical indicators, which could potentially be used to facilitate the individualized prediction of MSI status in patients with CRC.

## Key Points

- *There is an unmet need to non-invasively determine MSI status prior to treatment. However, the traditional radiological evaluation of CT is limited for evaluating MSI status.*
- *Our non-invasive CT imaging-based radiomics method could efficiently distinguish patients with high MSI disease from those with low MSI disease.*
- *Our radiomics approach demonstrated promising diagnostic efficiency for MSI status, similar to the commonly used IHC method.*

**Keywords** Colorectal cancer (CRC) · Microsatellite instability (MSI) · Polymerase chain reaction (PCR) · Nomogram · CT scans

---

Qian Pei and Xiaoping Yi contributed equally to this work.

---

✉ Xiaoping Yi  
yixiaoping@csu.edu.cn

✉ Qingling Li  
liqinglingw168@163.com

<sup>1</sup> Department of General Surgery, Xiangya Hospital, Central South University, Changsha, People's Republic of China

<sup>2</sup> Department of Radiology, Xiangya Hospital, Central South University, No. 87 Xiangya Road, Changsha 410008, People's Republic of China

<sup>3</sup> National Clinical Research Center for Geriatric Disorders (Xiangya Hospital), Central South University, Changsha 410008, People's Republic of China

<sup>4</sup> Department of Radiology, 331 Hospital of Zhuzhou City, Zhuzhou, People's Republic of China

<sup>5</sup> GE Healthcare, Hangzhou 310000, People's Republic of China

<sup>6</sup> Department of Pathology, Xiangya Hospital, Central South University, No. 87 Xiangya Road, Changsha 410008, People's Republic of China

<sup>7</sup> Department of Diagnostic Radiology, City of Hope National Medical Center, Duarte, CA, USA

## Abbreviations

AUC	Area under the curve
CRC	Colorectal cancer
CT	Computed tomography
dMMR	Deficient MMR
FFPE	Paraffin-embedded
HDL	High-density lipoprotein
ICCs	Inter-observer intraclass correlation coefficients
IHC	Immunohistochemistry
LASSO	Least absolute shrinkage and selection operator
MMR	Mismatch repair
MSI	Microsatellite instability
MSI-H	High MSI
MSI-L	Low MSI
MSS	Microsatellite stability
NCI	National Cancer Institute
PCR	Polymerase chain reaction
PLT	Platelet
pMMR	Proficient MMR
ROC	Receiver operating characteristic
ROI	Regions of interest

## Introduction

Colorectal cancer (CRC), ranking the third most common cancer and second most common cause of cancer-related death worldwide [1], is a highly heterogeneous disease driven by a series of genetic and epigenetic events [2]. Microsatellite instability (MSI), a consequence of a deficient DNA mismatch repair (MMR) system, is characterized by the generalized instability of short tandemly repeated DNA sequences known as microsatellites [3]. As one of the three major mechanisms of CRC carcinogenesis, MSI occurs in approximately 15% of CRC [3]. MSI has gained attention due to its values in diagnosis, treatment response, and prognosis of CRC [3–5].

There are several lines of evidence to support the use of pre-treatment MSI in clinical decision-making. First, MSI testing is recommended for the diagnosis of Lynch syndrome, the most common hereditary colon cancer syndrome, which is associated with germline mutations in one of the MMR genes (MLH1, MSH2, MSH6, or PMS2) [6]. MSI status helps to identify families with this syndrome and alerts the family members and relatives about their risk for this disease. Second, MSI is one of the key factors affecting the prognosis of CRC, especially for the early-stage cases [7, 8]. Patients with stage II CRC with high MSI (MSI-H)/deficient MMR (dMMR) usually have a more favorable prognosis than patients with microsatellite stability (MSS) and low MSI (MSI-L)/proficient MMR (pMMR) [8]. Third, MSI can be used to assess response to treatment, including fluoropyrimidine-based chemotherapy [9] and immunotherapy [10]. Fluoropyrimidine (5-FU or capecitabine) is the backbone of

the chemotherapeutic strategy for CRC, and it plays an important role in not only neoadjuvant therapy but also conversion therapy [11, 12]. However, patients with MSI-H status are generally resistant to 5-FU-based chemotherapy [13]. Immunotherapy is an emerging and promising therapy for CRC because MSI-H tumors have a large proportion of mutant neoantigens, which makes them sensitive to immune checkpoint inhibitors [14]. Therefore, MSI status is crucial for selecting CRC treatment and for evaluating response to treatment [15].

Currently, the diagnosis of MSI status relies on the collection of tissue specimens and molecular biology tests, such as the polymerase chain reaction (PCR) [3, 16], which is time-consuming and costly. In addition, tissue specimens for pre-treatment MSI testing are usually obtained by endoscopic biopsy, an invasive approach with potential risks for complications such as bleeding, bowel perfusion, and insufficient or inappropriate tissue sampling due to tumor heterogeneity. Therefore, there is an unmet need to non-invasively determine MSI status prior to treatment.

Computed tomography (CT) is the most widely used imaging method for CRC. However, it is challenging to identify MSI status based on the traditional radiological evaluation of routine CT images [2, 17]. Radiomics refers to the high-throughput computational extraction and analysis of imaging features from routine, clinically acquired radiological images. Radiomics can obtain potentially valuable high-dimensional information on tumor heterogeneity beyond the limitations of human eyes [18]. Prior studies [19, 20] have demonstrated the value of radiomics features as imaging predictors of diagnosis, treatment response, and prognosis in various cancers, including CRC [21, 22]. Three previous studies have presented the feasibility of using CT-based radiomics to predict MSI status for CRC [23–25]. However, all three studies had modest datasets ( $n = 102$ , or 119, or 198 respectively) and used the results of MMR immunohistochemistry (IHC) to label MSI status. IHC is a commonly used method to determine MSI status because of its feasibility and low cost [16]. However, compared to the gold standard PCR method, the IHC method has a high false-positive rate for CRC [4, 16]. Therefore, a non-invasive imaging-focused approach correlating with the more accurate PCR method may be helpful for determination of MSI status.

The current study aimed to assess radiomics features for predicting MSI status in patients with CRC who had their MSI status previously determined with the gold standard PCR method. We extracted radiomics features from clinically acquired abdominal pelvic CT scans. Our objective was to investigate the potential value of radiomics features in predicting MSI status for CRC patients before treatment. Such predictive information will be helpful for stratifying patients according to MSI status and for optimizing decision-making for personalized cancer treatment.

## Materials and methods

### Patients and data collection

This retrospective study was approved by the institutional review board at our hospital (IRB No. 201610070), and informed consent was waived due to the respective nature of this study.

We searched the database for consecutive patients with CRC confirmed by surgical pathology at our hospital between January 2013 and May 2019. The identification and selection of the study cohort, as well as exclusion criteria, are presented in Fig. 1.

Data regarding the demographics, clinical information, laboratory values, treatment details, outcome information, and CT scans were abstracted from medical records and reviewed by two clinicians (Q.P. and F.T.). Any discrepancy between the two clinicians was settled by a third clinician (H.Z.).

### Re-evaluation of pathology results

For each patient, all pathological slides for the CRC were re-analyzed by two pathologists who were specialized in gastrointestinal tumors (G.G. and Q.L. with 10 and 5 years of experience, respectively). Both pathologists were blinded to clinicopathological data. If any discrepancies arose, agreements were reached by consensus.

### MSI assessment

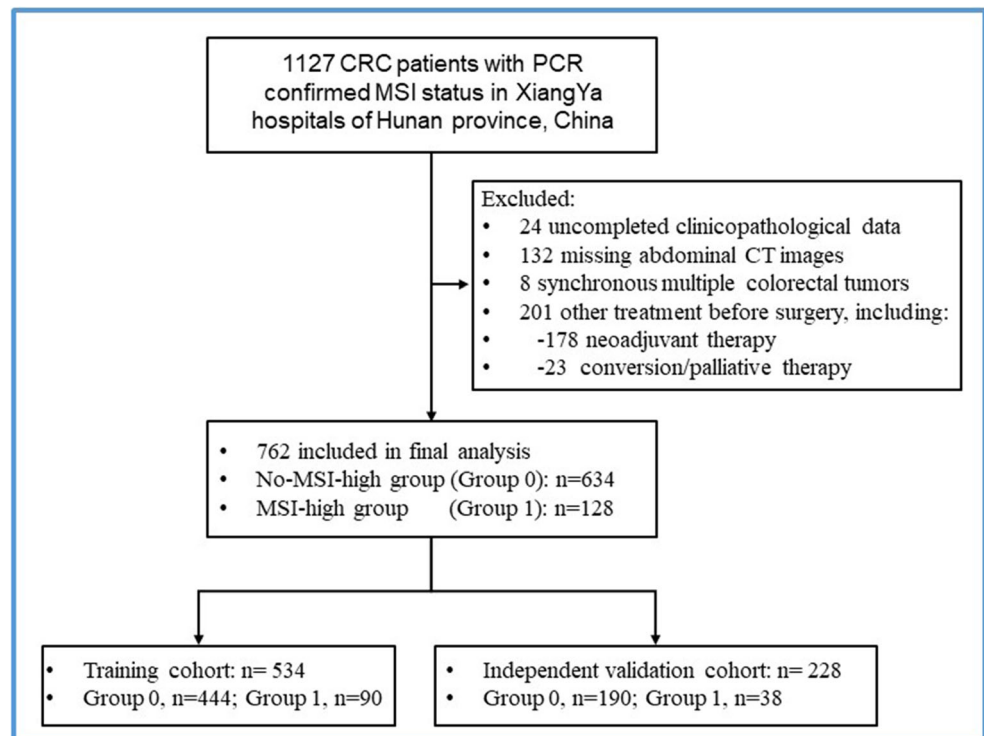
PCR method was used to determine MSI status with the DNA extracted from frozen or formalin-fixed, paraffin-embedded (FFPE) tumor tissue. The PCR determination was made according to the National Cancer Institute (NCI) panel consisting of two mononucleotide loci (BAT-25 and BAT-26) and three dinucleotide loci (D2S123, D5S346, and D17S250). Peripheral blood was analyzed as a positive control. The instability of two or more of these loci indicated MSI-H status. Instability of only one locus (MSI-L) and a lack of instability at any of the five loci were considered microsatellite stability (MSS) [3, 16].

For the IHC method [26], the expression of MMR proteins (MSH2, MSH6, MLH1, and PMS2) was identified using a standard streptavidin–biotin–peroxidase procedure [26]. Tumors displaying loss of any of the four MMR proteins upon nuclear staining were identified as dMMR and were MSI-H. Tumors with all four MMR proteins according to positive nuclear staining were identified as pMMR or non-MSI-H.

### CT image acquisition

Patients underwent routine CT scans of the abdomen and pelvis in one of the three CT scanners, i.e., a 16-MDCT (Brilliance 16, Philipps), a 64-MDCT (SOMATOM Definition, Siemens), and a 320-MDCT (Aquilion ONE, Toshiba Medical Systems) scanner. After an unenhanced

**Fig. 1** Flow-chart demonstrating patients' recruitment process for the present study



scan, a contrast-enhanced scan at the portal venous phase (scan with a fixed delay time of 60–70 s) was acquired. CT images including both the unenhanced images and the enhanced images at the portal venous phase were included in the analysis. All CT images were reconstructed with an axial thickness of 1 mm.

In order to remove the potential differences of CT images acquired from three different CT scanners, normalization with the final 256 bins was performed on all original CT images using the gray-scale discretization method before extracting the radiomics features (Analysis Kit software, version V3.0.0.R, GE Healthcare) [27].

### Radiomics feature extraction

CT images for each patient were reviewed independently by two abdominal radiologists (reader 1 [C.C.] and reader 2 [L.G.W.], with 15 and 25 years of experience, respectively) who were blinded to the patients' information. Any disagreements were resolved in a panel format with two additional readers (Y.X.P. and C.C.Y.). For each colorectal tumor, manual contouring and segmentation were performed on the axial images by both radiologists (readers 1 and 2) to define the tumor margins. The regions of interest (ROI) for tumor segmentation were saved for subsequent radiomics feature extraction using texture analytical software (MaZda Version 4.6, Institute of Electronics, Technical University of Lodz, Poland) [28]. For each CT image, a total of 340 quantitative texture features were automatically generated from each ROI file using MaZda software. The features included a gray level histogram, gradient, a run-length matrix, a co-occurrence matrix, an autoregressive model, and a wavelet transform analysis. The least absolute shrinkage and selection operator (LASSO) method was used for radiomics feature selection. Image analysis and prediction model construction are presented in Fig. 2.

### Reproducibility of radiomics feature extraction

The inter- and intra-observer reproducibility was initially assessed using 50 randomly selected CT images evaluated by two radiologists (reader 1 and reader 2). To assess intra-observer reproducibility, reader 1 generated texture features twice using the same procedure within a 2-week period. Generally, an intraclass correlation coefficient (ICC) greater than 0.75 is indicative of good agreement. Our inter- and intra-observer reproducibility of the radiomics feature extraction was satisfactory. The inter-observer ICC values of CT features extracted by reader 1 and reader 2 in their first extraction ranged from 0.772 to 0.864. The intra-observer ICC values for both extractions performed by reader 1 ranged from 0.807 to 0.924. As a result, all remaining cases were segmented by

reader 1 and the radiomics features were extracted for use in all subsequent calculations.

### Development of individualized prediction model

Multivariate logistic regression analysis was used to identify predictors of MSI. The nomogram for predicting MSI status was constructed with and without pathological features. Details can be found in the [Supplementary Files](#).

### Performance, validation, and preliminary clinical application of the nomogram

Calibration curves (Hosmer-Lemeshow H test) were used to evaluate the calibration of the nomogram, and receiver operating characteristic (ROC) curves were used to assess the diagnostic efficiency. To evaluate possible prediction errors using the proposed model in both cohorts, a 1000-iteration bootstrap analysis was conducted. The clinical usefulness of the nomogram was evaluated with decision curve analysis in the validation dataset.

To evaluate the diagnostic consistency between IHC method and nomogram developed in the present study (Fig. 3), the kappa consistency test was used. For the kappa consistency test, excellent, good, moderate, fair, and poor agreements were defined as kappa values of  $> 0.81$ , in the range of 0.61–0.80, 0.41–0.60, 0.21–0.40, and  $< 0.20$ , respectively.

### Statistical analysis

All statistical analysis was conducted using R software (version 3.5.2; <http://www.Rproject.org>). All statistical tests were two-sided, with statistical significance set at 0.05.

## Results

### Patient characteristics

A total of 762 patients with CRC were included in this study, including 128 with MSI-H status determined by the PCR analysis. Each patient was randomly assigned to the training cohort ( $n = 534$ ) or the validation cohort ( $n = 228$ ) at a ratio of 5:2 (Fig. 1).

Patient characteristics and a comparison between patients with MSI-H or no-MSI-H disease are presented in Table 1. Significant differences between the cohorts were found in patient age, presence of a comorbidity (hypertension), tumor location, laboratory markers (routine blood test and blood fat metabolism data), and pathology (subtype and M stage) (Table 1). Briefly, when compared to no-MSI-H patients, patients with MSI-H status

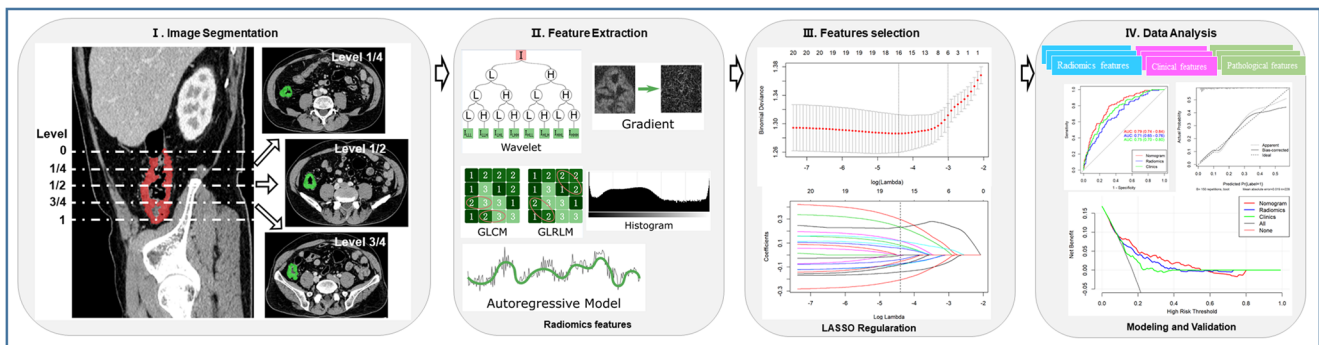


**Fig. 2** Workflow for radiomics data extraction, feature reduction, and modeling performed for this study. (I) Tumor segmentation on CT images. Three representative cross-sectional images were selected for tumor contouring. (II) Strategy for extracting radiomics data from CT images. Radiomics features were extracted from the tumor contours for tumor histogram, autoregressive model, GLCM, GLRLM, gradient, and wavelet texture. (III) Least absolute shrinkage and selection operator (LASSO)

were younger and had a higher incidence of concurrent hypertension, higher platelet (PLT), and lower expression of high-density lipoprotein (HDL). No variables were statistically different between the training and the validation cohorts ( $p > 0.05$ ), ensuring a reasonable classification.

### Feature selection and radiomics signature

Of all the radiomics features, those with non-zero coefficients in the least absolute shrinkage and selection operator (LASSO) logistic regression model were selected to build the differentiation model. After dimensionality reduction, a total of 16 potential predictors were selected from the 352 features performed in the training cohort ( $n = 634$  patients, Supplementary Figure 1 and Figure 2). An equation was developed to yield a new radiomics signature termed Rad-score (Supplementary Files).

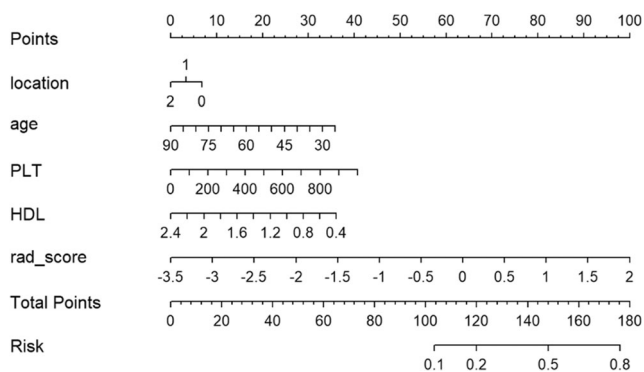


**Fig. 3** Development of radiomics nomogram. Radiomics nomogram was developed in the training cohort incorporating the radiomics signature, platelet (PLT) and high-density lipid (HDL) values, age, and tumor location

method used for radiomics feature reduction. (IV) Prediction model constructed with multivariate logistic regression based on radiomics, clinical, and pathological features. Receiver operating characteristic (ROC) and calibration curves applied to assess the model performance. Decision curve analysis was performed to evaluate the clinical value of the prediction models

### Diagnostic performance of radiomics signature

The distribution of Rad-scores with regard to MSI status in the training and validation cohorts is presented in Supplementary Figure 3. In the training cohort, patients from the MSI-H group generally had a much higher Rad-score than those with no-MSI-H status ( $p < 0.001$ ), which was confirmed in the validation cohort ( $p < 0.001$ ). The Rad-score yielded a C-index of 0.70 (95% CI, 0.64–0.76) for the training cohort and 0.72 (95% CI, 0.63–0.82) for the validation cohort (Fig. 4a, b).

### Development of individualized MSI prediction model

All parameters with  $p$  values less than 0.05 from the univariate analysis were carried forward into the multivariate regression analysis. The radiomics model was constructed using multivariate logistic regression analysis method. Backward stepwise selection was applied by using the likelihood ratio test with Akaike's information criterion as the stopping rule to select correlated factors of MSI-H.

Finally, the rad-score, PLT, HDL level, age, and tumor location were identified as independent predictors of MSI status. A nomogram was subsequently developed by incorporating the above independent predictors (Fig. 3).

### Performance and validation of prediction models

The calibration curve of the nomogram about the two groups for probabilities of MSI-H status demonstrated the predicted values being in good agreement with the observed values (Fig. 4c, d). The Hosmer-Lemeshow H test showed that the statistical results in the training group ( $p = 0.267$ ) and the verification group ( $p = 0.145$ ) were not significant, indicating that there was no deviation from the perfect fit. The radiomics model achieved a moderate efficiency with an area under the

**Table 1** Demographic, clinical, laboratory, pathologic, and radiomics characteristics of 762 patients with colorectal cancer (CRC) and their microsatellite instability (MSI) status

Characteristic	Total (n = 762)	MSI-H (n = 128)	Non-MSI-H (n = 634)	p value	Training cohort (n = 534)	Validation cohort (n = 228)	p value
<b>Demographics and clinical characteristics</b>							
Gender, n (%)							
Male	439 (57.61)	70 (54.69)	369 (58.20)	0.463	308 (57.68)	131 (57.46)	0.955
Female	323 (42.39)	58 (45.31)	265 (41.80)		226 (42.32)	97 (42.54)	
Age (y)	57 (48–66)	52 (45–63)	59 (49–67)	< 0.001***	57.00 (48.75–66.00)	58.00 (48.25–67.00)	0.438
Smoking, n (%)							
Yes	280 (36.75)	44 (34.38)	236 (37.22)	0.542	205 (38.39)	75 (32.89)	0.150
No	482 (63.25)	84 (65.63)	398 (62.780)		329 (61.61)	153 (67.11)	
Alcohol, n (%)							
Yes	224 (29.40)	36 (28.13)	188 (39.65)	0.729	160 (29.96)	64 (28.07)	0.600
No	538 (70.60)	92 (71.88)	446 (70.35)		374 (70.04)	164 (71.93)	
Family history of cancer, n (%)							
Yes	76 (9.97)	18 (14.06)	58 (9.15)	0.091	51 (9.55)	25 (10.96)	0.551
No	686 (90.03)	110 (85.94)	576 (90.85)		483 (90.45)	203 (89.04)	
Diabetes, n (%)							
Yes	83 (10.89)	10 (7.81)	73 (11.51)	0.220	60 (11.24)	23 (10.09)	0.641
No	679 (89.11)	118 (92.19)	561 (88.49)		474 (88.76)	205 (89.91)	
Hypertension, n (%)							
Yes	182 (23.88)	18 (14.06)	164 (25.87)	0.004**	126 (23.60)	56 (24.56)	0.775
No	580 (76.12)	110 (85.94)	470 (74.13)		408 (76.40)	172 (75.44)	
Infectious disease, n (%)							
HBV	64 (8.40)	7 (5.47)	57 (8.99)	0.372	45 (8.43)	19 (8.33)	0.631
HCV	3 (0.39)	0 (0)	3 (0.47)		1 (0.19)	2 (0.88)	
Syphilis	20 (2.62)	3 (2.34)	17 (2.68)		14 (2.62)	6 (2.63)	
No	675 (88.58)	118 (92.19)	557 (87.85)		474 (88.76)	201 (88.16)	
Tumor location, n (%)							
Right colon	270 (35.43)	71 (55.47)	199 (31.39)	< 0.001***	193 (36.14)	77 (33.77)	0.246
Left colon	235 (30.84)	38 (29.69)	197 (31.07)		155 (29.03)	80 (35.09)	
Rectum	257 (33.73)	19 (14.84)	238 (37.54)		186 (34.83)	71 (31.14)	
<b>Laboratory findings</b>							
Positive OB test of stool, n (%)							
Yes	673 (88.32)	114 (89.06)	559 (88.17)	0.774	476 (89.14)	197 (86.40)	0.282
No	89 (11.68)	14 (10.94)	75 (11.83)		58 (10.86)	31 (13.60)	
Blood routine test							
WBC (10 <sup>9</sup> /L)	6.30 (5.10–7.60)	6.55 (5.10–8.20)	6.20 (5.10–7.50)	0.158	6.30 (5.20–7.60)	6.30 (5.03–7.50)	0.652
RBC (10 <sup>9</sup> /L)	4.32 ± 0.63	4.19 ± 0.64	4.34 ± 0.63	0.012*	4.34 ± 0.63	4.27 ± 0.62	0.168
HGB (g/L)	125 (107–139)	115 (92–134)	128 (110–140)	< 0.001***	125.50 (108.00–139.25)	125.00 (101.75–138.00)	0.377
PLT (10 <sup>9</sup> /L)	250 (203–311)	285.50 (227.25–355.50)	243.50 (200.75–303.00)	< 0.001***	252.00 (203.00–312.25)	243.00 (201.25–305.75)	0.498
Neutrophil (10 <sup>9</sup> /L)	3.90 (3.10–4.90)	4.20 (3.10–5.60)	3.80 (3.00–4.80)	0.033*	3.90 (3.10–4.93)	3.80 (3.00–4.90)	0.727
Lymphocyte (10 <sup>9</sup> /L)	1.60 (1.30–2.00)	1.50 (1.20–1.80)	1.60 (1.30–2.00)	0.230	1.60 (1.30–2.00)	1.50 (1.20–2.00)	0.061
Monocyte (10 <sup>9</sup> /L)	0.50 (0.40–0.60)	0.50 (0.40–0.67)	0.50 (0.40–0.60)	0.085	0.50 (0.40–0.60)	0.50 (0.40–0.600)	0.886
RDW (%)	13.50 (12.80–14.90)	13.80 (13.10–15.88)	13.45 (12.70–14.70)	0.007**	13.50 (12.70–14.80)	13.55 (12.80–15.20)	0.486
PCT (%)	0.25 (0.20–0.30)	0.28 (0.22–0.35)	0.24 (0.20–0.30)	< 0.001***	0.25 (0.20–0.31)	0.24 (0.20–0.30)	0.074
MPV (fl)	9.90 (8.88–10.90)	9.50 (8.52–10.77)	10.00 (8.90–10.90)	0.035	10.00 (8.91–11.00)	9.70 (8.70–10.53)	0.014*
NLR	2.33 (1.74–3.33)	2.61 (1.96–3.70)	2.29 (1.71–3.27)	0.007**	2.32 (1.73–3.23)	2.36 (1.77–3.53)	0.386
Liver function test							
Albumin (g/L)	41.35 (38.18–44.20)	40.60 (37.10–43.68)	41.40 (38.40–44.53)	0.067	41.30 (38.40–44.10)	41.40 (37.73–44.68)	0.918
Globulin (g/L)	27.50 (24.70–30.20)	27.10 (24.50–30.15)	27.50 (24.80–30.20)	0.659	27.50 (24.80–30.53)	27.15 (24.50–29.80)	0.396
A/G ratio	1.52 ± 0.30	1.50 ± 0.32	1.53 ± 0.30	0.407	1.52 ± 0.30	1.54 ± 0.30	0.471
Blood glucose (mmol/L)	5.23 (4.73–5.77)	5.16 (4.65–5.72)	5.24 (4.74–5.78)	0.682	5.21 (4.73–5.75)	5.27 (4.74–5.85)	0.358
Lipid metabolism in serum							
TG (mmol/L)	1.38 (1.06–1.51)	1.37 (1.08–1.52)	1.43 (1.05–1.51)	0.384	1.38 (1.07–1.49)	1.38 (1.03–1.55)	0.963
Cholesterol (mmol/L)	4.69 (4.20–5.04)	4.54 (4.08–4.87)	4.69 (4.20–5.11)	0.003**	4.69 (4.22–5.08)	4.69 (4.13–5.01)	0.704
HDL (mmol/L)	1.19 (1.02–1.30)	1.12 (1.00–1.25)	1.19 (1.02–1.30)	0.026*	1.19 (1.02–1.29)	1.19 (1.01–1.32)	0.674
LDL (mmol/L)	2.93 (2.53–3.20)	2.83 (2.50–3.08)	2.93 (2.54–3.22)	0.022*	2.93 (2.56–3.22)	2.92 (2.50–3.17)	0.320

**Table 1** (continued)

Characteristic	Total (n = 762)	MSI-H (n = 128)	Non-MSI-H (n = 634)	p value	Training cohort (n = 534)	Validation cohort (n = 228)	p value
Serum tumor markers							
CEA (ng/mL)	2.62 (1.29–7.46)	2.29 (1.28–5.79)	2.72 (1.29–8.35)	0.133	2.53 (1.22–7.46)	2.75 (1.35–7.46)	0.333
CA199 (U/mL)	9.67 (5.23–23.10)	10.03 (5.11–25.45)	9.67 (5.25–21.83)	0.676	9.66 (5.14–23.44)	10.32 (5.51–22.17)	0.543
CA125 (U/mL)	6.63 (4.16–11.45)	6.81 (4.39–13.10)	6.63 (4.02–11.19)	0.178	6.47 (3.97–11.48)	6.94 (4.70–11.24)	0.286
Pathological characteristics							
Pathological type, n (%)							
Well differentiated adenocarcinoma	551 (72.31)	68 (53.13)	483 (76.18)	< 0.001***	386 (72.28)	165 (72.37)	0.663
Poorly differentiated adenocarcinoma	99 (12.99)	26 (20.31)	73 (11.51)		73 (13.67)	26 (11.40)	
Mucinous carcinoma	22 (2.89)	6 (4.69)	16 (2.52)		16 (3.00)	6 (2.63)	
Mixed carcinoma	90 (11.81)	28 (21.88)	62 (9.78)		59 (11.05)	31 (13.60)	
T stage, n (%)							
T1	17 (2.23)	2 (1.56)	15 (2.37)	0.528	8 (1.50)	9 (3.95)	0.186
T2	88 (11.55)	13 (10.16)	75 (11.83)		60 (11.24)	28 (12.28)	
T3	596 (78.22)	106 (82.81)	490 (77.29)		424 (79.40)	172 (75.44)	
T4	61 (8.01)	7 (5.47)	54 (8.52)		42 (7.87)	19 (8.33)	
N stage, n (%)							
N0	482 (63.25)	89 (69.53)	393 (61.99)	0.266	333 (62.36)	149 (65.35)	0.731
N1	175 (22.97)	25 (19.53)	150 (23.66)		126 (23.60)	49 (21.49)	
N2	105 (13.78)	14 (10.94)	91 (14.35)		75 (14.04)	30 (13.16)	
M stage, n (%)							
M0	678 (88.98)	124 (96.88)	554 (87.38)	0.002**	474 (88.76)	204 (89.47)	0.775
M1	84 (11.02)	4 (3.13)	80 (12.62)		60 (11.24)	24 (10.53)	
CT-based radiomics							
Rad-score	−0.42 (−3.04–1.66)	0.08 (−2.34–1.67)	−0.49 (−3.04–1.47)	< 0.001***	−0.46 (−3.04–1.67)	−0.35 (−2.07–1.47)	0.061

**Note.**—Unless otherwise indicated, data are numbers of patients, and data in parentheses are percentages. \* $p < 0.05$ , \*\* $p < 0.01$ , and \*\*\* $p < 0.001$  suggest a significant difference between the characteristics in the two cohorts. *HDL*, chronic obstructive pulmonary disease

curve (AUC) of 0.74 (95% CI: 0.68–0.80) for the training cohort, and 0.77 (95% CI: 0.68–0.85) for the validation cohort, respectively (Fig. 4a, b), as well as a good performance of consistence (bootstrap for the training cohort:  $0.75 \pm 0.04$ ; for the validation cohort:  $0.74 \pm 0.03$ ).

### Predictive performance of radiomics nomogram with addition of pathological characteristics

The differentiation nomogram after adding pathological characteristics is shown in Supplementary Figure 4 (A). The calibration curve for the probability of MSI-H status in the training and validation cohorts showed good agreement between prediction and observation (Supplementary Figure 4B and 4C). A slightly higher AUC was observed for the new model after integrating pathological characteristics both in the training cohort (0.79; 95% CI: 0.74 to 0.84) and in the validation cohort (0.74; 95% CI: 0.65 to 0.83) (Fig. 4a, b). Nevertheless, incorporation of the pathological characteristics into the prediction model did not show significantly improved prediction efficiency ( $p > 0.05$ ).

### Clinical application

The decision curve analysis of the nomogram is presented in Fig. 5. The decision curve showed that if the threshold probability of a user was greater than 10%, then using the nomogram to predict MSI-H status in CRC patients may add more benefit than using either the diagnose-all MSI-patients scheme or the diagnose-none MSI scheme alone. However, using the combined models showed no additional clinical benefit compared to using the clinical model alone.

### Comparison of diagnostic performance between the nomogram and IHC method

A total of 336 cases had MSI results determined by the IHC method. Evaluation of diagnostic consistency showed a fair consistency ( $\kappa = 0.34$ ) between the nomogram and the IHC method. The IHC method in this cohort showed a sensitivity of 60.29% (95% CI: 60.18–60.41%) and a specificity of 94.78% (95% CI: 94.75–94.80%). On the contrary, our nomogram demonstrated a much higher

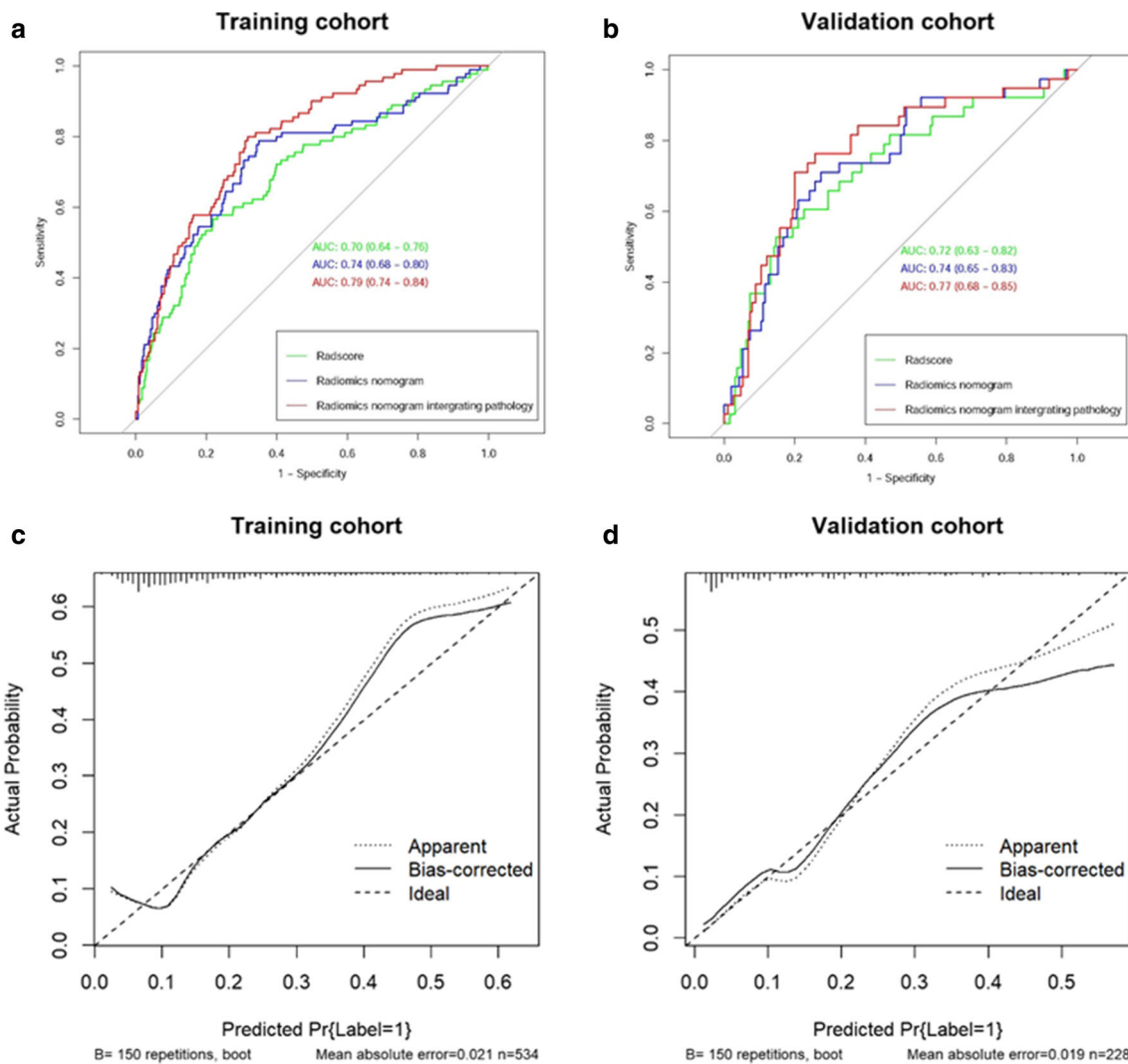


**Fig. 4** Receiver operating characteristic (ROC) curves for training (a) and independent validation (b) for three models: radiomics signature only (Rad-score), and radiomics model incorporating without or with pathological characteristics (combined). The area under the curve (AUC) for

three models was demonstrated on the corresponding figure respectively. Calibration curves of the radiomics nomogram in the training cohort (c) and the validation cohort (d). Calibration curves showed the calibration of the predictive model for the risk of MSI-H disease

sensitivity (80.00%, 95% CI: 70.20–87.71%) but a lower specificity (68.69%, 95% CI: 63.90–72.82%). A series of parallel diagnostic experiments could not obviously improve the sensitivity of the IHC method (57.35%, 95% CI: 57.24–57.47%) or specificity of the nomogram (67.91%, 95% CI: 67.86–67.97%).

**Discussion**

We developed a radiomics nomogram using clinically acquired abdominal pelvic CT images from 762 patients with CRC at a single center. Our study results indicated the potential of this radiomics method as a tool for evaluating MSI status in clinical practice. Radiomics features derived from pre-treatment CT images were found to be associated with

MSI status in patients with CRC. A model combining radiomics features and clinical variables could efficiently separate those with MSI-H disease from those with MSS disease. Our study emphasized the relevance of the computational radiomics analysis of pre-treatment CT images for comprehensive evaluation of tumor heterogeneity in patients with CRC before surgery. To the best of our knowledge, among all the reported radiomics studies for predicting MSI status in CRC, our study was the first to build prediction models correlating the PCR results from untreated surgical specimen with radiomics features.

The prediction efficiency of our model may appear to be lower than that of the previous models judging by the AUC value (our: 0.74 versus others’: 0.75, 0.80, 0.96, respectively) [23–25]. However, it is challenging to directly compare the predictive power of our approach to others. Although our



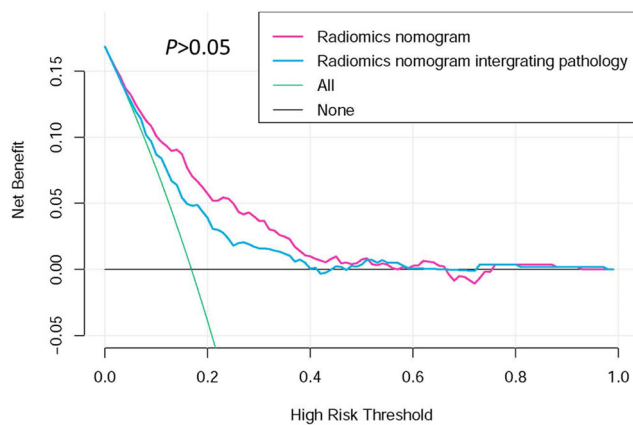


**Fig. 5** Decision curve analysis for the Rad-score, radiomics nomogram, and combined model. The y-axis measures the net benefit. The blue line and the pink line represent the radiomics nomogram without or with the pathological features, respectively. The black line represents the assumption that no patients would develop MSI-H disease, and the green line represents the assumption that all patients would develop MSI-H disease

study used CT-based radiomics to predict MSC status in CRC in a similar way as the previous studies, we used the results from the gold standard PCR method which should reflect more accurate MSI status while the other studies used the MMR immunohistochemistry (IHC) method. The shortcomings of the IHC method include a high false-positive rate and high dependence on the quality of specimens which typically exhibit a gradual loss of nucleic acids or proteins over time [3, 16]. In addition, our study had a larger sample size with over 700 patients while the previous studies all had modest sample size ranging from 102 to 198 patients. In our cohort, a subsequent diagnostic consistency test showed that there was satisfying performance when comparing the diagnostic performance of the radiomics approach and the IHC method. This suggested that our model may have the potential to be used as a non-invasive method for testing MSI status.

Our results showed the potential value of CT radiomics features for assessing genetic information for CRC [23, 24]. Although the underlying mechanism for radiomics reflecting MSI status remains unclear, we speculate that radiomics may represent tumor heterogeneity and thus predict genetic alterations [18, 20, 29]. Tumor heterogeneity can be assessed at histological level, which may be the result of potential genetic changes [30], and has been reported to be associated with MSI status in CRC. Previous studies have reported that CRC tumors with MSI-H tend to be well or poorly differentiated, being mucinous, having increased tumor-infiltrating lymphocytes, having a circumscribed or expansile growth pattern, showing histologic heterogeneity, and having a prominent Crohn-like reaction at the advancing edge of the tumor [31]. These pathological features suggest that the heterogeneity of MSI-H tumors may be higher than that of no-MSI-H tumors histologically, which could be captured on imaging using

radiomics. In our study, SumEntrp and SumOfSqs as co-occurrence matrix features were ranked as the top two of all radiomics features. It appeared as the larger values of SumEntrp and SumOfSqs may reflect greater spatial heterogeneity of tumor on imaging. According to the equation for the rad-score developed in this study, tumors with these features tended to be MSI-H, which was consistent with the findings of previous studies [24, 32]. Therefore, we should not be surprised to see the association between radiomics features and MSI status in our study.

The radiomics approach of utilizing existing clinical images to capture tumor heterogeneity may be used to develop a non-invasive imaging biomarker to predict MSI status before treatment. Currently, clinical CT scans are routinely obtained for diagnosis and staging but not for MSI identification [2]. However, these routine CT images contain important information reflecting the characteristics of the entire tumor heterogeneity including the biological information determined by the underlying protein, gene, and other micro-level components of the tumor tissue [17, 19, 20]. Although these high-dimensional imaging features are not discernable by the human eye, computational radiomics analysis can decipher them in a meaningful way to potentially assist clinicians in decision-making [18]. MSI status has been shown to be statistically associated with pathological features such as tumor types (mucinous carcinoma or not), differentiation, lymphatic invasion, and tumor staging [3, 33]. Our study did not show significant improvement of model performance after addition of pathological features to the radiomics nomogram. Our study result implicated the independent value of pre-treatment CT-based radiomics in predicting MSI status for patients with CRC.

Our radiomics method has unique advantages. First, the imaging data was stored and could be used repeatedly, which was an advantage over using biological specimens. Second, MSI prediction may be further improved over time through trial and error of various advanced methods including machine learning algorithms and artificial intelligence. Moreover, without the additional cost for the PCR and IHC methods, the radiomics method may improve the cost-effectiveness ratio. Our study results suggested that the pre-treatment CT image-based radiomics approach has the potential to non-invasively predict tumor MSI status with promising efficiency before treatment with surgery, chemotherapy, or chemoradiotherapy. Nevertheless, we should be cognizant of the disadvantages associated with the radiomics method. For instance, manual tumor segmentation step in the radiomics analysis could be time-consuming and burdensome for busy clinicians. In addition, the issues with CT tumor conspicuity may also pose additional challenges for analyzing the imaging data. Development of accurate automatic or semi-automatic segmentation methods may help to ease the adaptation of radiomics into clinical practice.

Among the four clinical indicators identified in the present study, tumor location was the only one which has already been reported as a clinical indicator in literature [33]. We found that tumors located in the right-sided colon were more likely to be MSI-H, whereas rectal cancer was inclined to be MSS. We also observed that younger CRC patients usually had a higher incidence of MSI-H, which was consistent with published literature [34]. We identified two of peripheral blood parameters, PLT and HDL, as significant indicators, which have not yet been reported. Apart from their well-described crucial function in hemostasis, platelets have been shown to play important roles in cancer growth, metastasis, and immune evasion [35]. Activated platelets in the tumor microenvironment promote cancer cell escape from immune recognition. It has been known that tumors including CRC with MSI-H exist in a microenvironment of richly repressed immune cells such as T-cells and NK cells [36]. It is plausible to speculate that MSI-H CRC cells may stimulate the production of platelets, recruit the platelets to the tumor microenvironment, and help to evade immune surveillance. HDL-related lipids and proteins, which were first recognized as anti-atherosclerotic based on their role in reverse cholesterol transport, typically exhibit diverse functions in oxidative stress, inflammation, immunity, and tumorigenesis [37]. However, the relationship between HDL, cancer incidence, and mortality is not clear and may be tumor dependent. So far, there has been limited research on the association between HDL and MSI status. Our study provided a new research direction to explore since lipid metabolism and lifestyle modifications have been known to be important modifiable variables for CRC.

There were limitations to the study. First, the retrospective nature of this single-center study may lead to inevitable case selection bias, as well as limited generalizability. Second, although a relatively large number of CRC patients ( $n=762$ ) were included in our study, this cohort was still small considering the high incidence of CRC, which may affect the general applicability of our results. A large-scale, prospective, multi-center study is needed to validate our results. Last, our study was limited with potential overfitting issues. We used 16 radiomics features and 20 features in total when combined with clinical features for modeling. The number of cases per feature was far from ideal and there was a potential for the model being over-fitted. This was especially serious for the minority class of 90 with only 4.5 cases per feature, below the 10 patients required to test one feature optimally, which may result in overfitting the models.”

In summary, we presented a non-invasive radiomics approach utilizing clinically acquired CT images to identify MSI status in patients with CRC prior to treatment. The information from the current study could potentially be used to assist clinical decision-making for personalized treatment of CRC.

**Supplementary Information** The online version contains supplementary material available at <https://doi.org/10.1007/s00330-021-08167-3>.

**Acknowledgements** We thank Dr. Feiyue Zeng (Xiangya Hospital, Central South University) for helpful discussion and assistance in data analysis. We thank staff members in the Departments of Radiology, General Surgery, and Pathology at Xiangya Hospital for their efforts in collecting the information used in this study. Editing assistance was provided by Kerin Higa, PhD (City of Hope National Medical Center).

**Funding** This study has received funding (in part) by the Natural Science Foundation of Hunan Province (2018JJ2641).

## Declarations

**Guarantor** The scientific guarantor of this publication is Prof. Xiaoping Yi.

**Conflict of interest** One of the authors of this manuscript (Peipei Pang) is an employee of GE Healthcare. The remaining authors declare no relationships with any companies whose products or services may be related to the subject matter of the article.

**Statistics and biometry** One of the authors has significant statistical expertise.

**Informed consent** Written informed consent was waived by the Institutional Review Board.

**Ethical approval** Institutional Review Board approval was obtained.

## Methodology

- Retrospective
- Case-control study
- Performed at one institution

## References

1. Ferlay J, Colombet M, Soerjomataram I et al (2019) Estimating the global cancer incidence and mortality in 2018: GLOBOCAN sources and methods. *Int J Cancer* 144:1941–1953
2. Dekker E, Tanis PJ, Vleugels JLA, Kasi PM, Wallace MB (2019) Colorectal cancer. *Lancet* 394:1467–1480
3. Kawakami H, Zaanani A, Sinicrope FA (2015) Microsatellite instability testing and its role in the management of colorectal cancer. *Curr Treat Options Oncol* 16:30
4. Evrard C, Tachon G, Randrian V, Karayan-Tapon L, Tougeron D (2019) Microsatellite instability: diagnosis, heterogeneity, discordance, and clinical impact in colorectal cancer. *Cancers (Basel)* 11(10):1567
5. Liu W, Zhang D, Tan SA, Liu X, Lai J (2018) Sigmoid colon adenocarcinoma with isolated loss of PMS2 presenting in a patient with synchronous prostate cancer with intact MMR: Diagnosis and Analysis of the Family Pedigree. *Anticancer Res* 38:4847–4852
6. Vasen HF (2005) Clinical description of the Lynch syndrome [hereditary nonpolyposis colorectal cancer (HNPCC)]. *Fam Cancer* 4: 219–225
7. Popat S, Hubner R, Houlston RS (2005) Systematic review of microsatellite instability and colorectal cancer prognosis. *J Clin Oncol* 23:609–618

8. Merok MA, Ahlquist T, Røyrvik EC et al (2013) Microsatellite instability has a positive prognostic impact on stage II colorectal cancer after complete resection: results from a large, consecutive Norwegian series. *Ann Oncol* 24:1274–1282
9. Li LS, Morales JC, Veigl M et al (2009) DNA mismatch repair (MMR)-dependent 5-fluorouracil cytotoxicity and the potential for new therapeutic targets. *Br J Pharmacol* 158:679–692
10. Mandal R, Samstein RM, Lee KW et al (2019) Genetic diversity of tumors with mismatch repair deficiency influences anti-PD-1 immunotherapy response. *Science* 364:485–491
11. Ludmir EB, Palta M, Willett CG, Czito BG (2017) Total neoadjuvant therapy for rectal cancer: an emerging option. *Cancer* 123:1497–1506
12. Tomasello G, Petrelli F, Ghidini M, Russo A, Passalacqua R, Barni S (2017) FOLFOXIRI plus bevacizumab as conversion therapy for patients with initially unresectable metastatic colorectal cancer: a systematic review and pooled analysis. *JAMA Oncol* 3:e170278
13. Fischer F, Baerenfaller K, Jiricny J (2007) 5-Fluorouracil is efficiently removed from DNA by the base excision and mismatch repair systems. *Gastroenterology* 133:1858–1868
14. Chalabi M, Fanchi LF, Dijkstra KK et al (2020) Neoadjuvant immunotherapy leads to pathological responses in MMR-proficient and MMR-deficient early-stage colon cancers. *Nat Med* 26:566–576
15. Diagnosis And Treatment Guidelines For Colorectal Cancer Working Group CSOCOC (2019) Chinese Society of Clinical Oncology (CSCO) diagnosis and treatment guidelines for colorectal cancer 2018 (English version). *Chin J Cancer Res* 31:117–134
16. Harada S, Morlote D (2020) Molecular pathology of colorectal cancer. *Adv Anat Pathol* 27:20–26
17. Gillies RJ, Kinahan PE, Hricak H (2016) Radiomics: Images Are More than Pictures, They Are Data. *Radiology* 278:563–577
18. Gardin I, Gregoire V, Gibon D et al (2019) Radiomics: principles and radiotherapy applications. *Crit Rev Oncol Hematol* 138:44–50
19. Yi X, Guan X, Zhang Y et al (2018) Radiomics improves efficiency for differentiating subclinical pheochromocytoma from lipid-poor adenoma: a predictive, preventive and personalized medical approach in adrenal incidentalomas. *EPMA J* 9:421–429
20. Rogers W, Thulasi SS, TAG R et al (2020) Radiomics: from qualitative to quantitative imaging. *Br J Radiol* 93:20190948
21. Badic B, Hatt M, Durand S et al (2019) Radiogenomics-based cancer prognosis in colorectal cancer. *Sci Rep* 9:9743
22. Yi X, Pei Q, Zhang Y et al (2019) MRI-based radiomics predicts tumor response to neoadjuvant chemoradiotherapy in locally advanced rectal cancer. *Front Oncol* 9:552
23. Wu J, Zhang Q, Zhao Y et al (2019) Radiomics analysis of iodine-based material decomposition images with dual-energy computed tomography imaging for preoperatively predicting microsatellite instability status in colorectal cancer. *Front Oncol* 9:1250
24. Golia PJS, Gagniere J, Chakraborty J et al (2019) Radiomics-based prediction of microsatellite instability in colorectal cancer at initial computed tomography evaluation. *Abdom Radiol (NY)* 44:3755–3763
25. Fan S, Li X, Cui X et al (2019) Computed tomography-based radiomic features could potentially predict microsatellite instability status in stage II colorectal cancer: a preliminary study. *Acad Radiol* 26:1633–1640
26. Lindor NM, Burgart LJ, Leontovich O et al (2002) Immunohistochemistry versus microsatellite instability testing in phenotyping colorectal tumors. *J Clin Oncol* 20:1043–1048
27. Gao C, Yan J, Luo Y et al (2020) The growth trend predictions in pulmonary ground glass nodules based on radiomic CT features. *Front Oncol* 10:580809
28. Szczypiński PM, Strzelecki M, Materka A, Klepaczko A (2009) MaZda—a software package for image texture analysis. *Comput Methods Programs Biomed* 94:66–76
29. Forghani R, Savadjiev P, Chatterjee A, Muthukrishnan N, Reinhold C, Forghani B (2019) Radiomics and artificial intelligence for biomarker and prediction model development in oncology. *Comput Struct Biotechnol J* 17:995–1008
30. Yi X, Liu Y, Zhou B et al (2021) Incorporating SULF1 polymorphisms in a pretreatment CT-based radiomic model for predicting platinum resistance in ovarian cancer treatment. *Biomed Pharmacother* 133:111013
31. Greenson JK, Huang SC, Herron C et al (2009) Pathologic predictors of microsatellite instability in colorectal cancer. *Am J Surg Pathol* 33:126–133
32. Dercle L, Lu L, Schwartz LH et al (2020) Radiomics response signature for identification of metastatic colorectal cancer sensitive to therapies targeting EGFR pathway. *J Natl Cancer Inst* 112(9):902–912
33. Boland CR, Goel A (2010) Microsatellite instability in colorectal cancer. *Gastroenterology* 138:2073–2087.e3
34. Song Y, Wang L, Ran W et al (2020) Effect of tumor location on clinicopathological and molecular markers in colorectal cancer in Eastern China patients: an analysis of 2,356 cases. *Front Genet* 11:96
35. Gaertner F, Massberg S (2019) Patrolling the vascular borders: platelets in immunity to infection and cancer. *Nat Rev Immunol* 19:747–760
36. Payandeh Z, Oho AUID, Khalili S et al (2020) PD-1/PD-L1-dependent immune response in colorectal cancer. *J Cell Physiol* 235:5461–5475
37. Ganjali S, Ricciuti B, Pirro M et al (2019) High-Density Lipoprotein Components and Functionality in Cancer: State-of-the-Art. *Trends Endocrinol Metab* 30:12–24

**Publisher's note** Springer Nature remains neutral with regard to jurisdictional claims in published maps and institutional affiliations.